The Abdus Salam
International Centre for Theoretical Physics

United Nations
Educational, Scientific and
Cultural Organization

IAEA
International Atomic Energy Agency

SMR/1842-1

International Workshop on QCD at Cosmic Energies III

28 May - 1 June, 2007

report (sarycheva)

L. Sarycheva
Lomonosov Moscow State University
Moscow, Russia

Prospects for studies of exotic phenomena at LHC

L.I.Sarycheva

Moscow State University
Scobeltsyn Institute of Nuclear Physics
Moscow, Russia, 119992

Contents

1. Investigation of Alignment Fenomenon for CMS at LHC

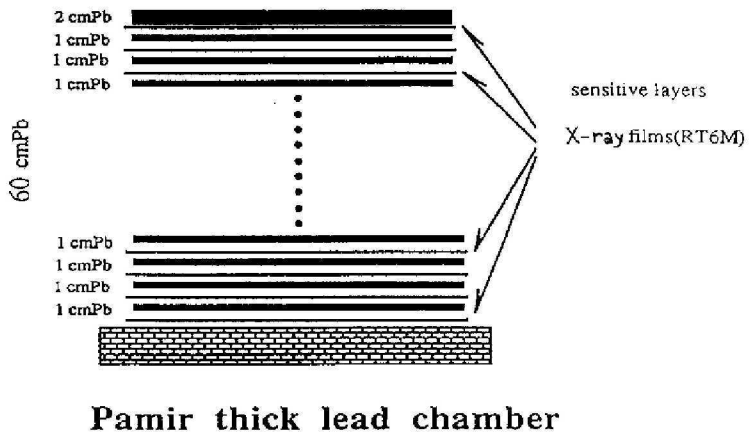

FIG. 1. Structure of the most-used deep lead chamber of 60 cm thickness from Pamir experiment.

As an alignment criterion the parameter of asymmetry introduced by Borisov is conventionally used:

$$\lambda_m = \frac{\sum\limits_{i\neq j\neq k=1}^{m} \cos 2\varphi_{ijk}}{m(m-1)(m-2)}.$$

Here m is the number of objects, i, j, k stand for vertices, and φ_{ijk} is the angle between two vectors $\vec{ki}$ and $\vec{kj}$.

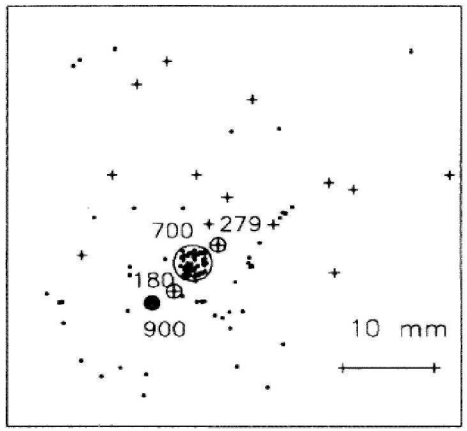

FIG. 2. An example of the target diagram with energy distinguished cores for the event with alignment (the family Pb-6). λ_4=0.95. Figures in the plot stand for energy in TeV (already multiplied by 3 for hadrons). EDC: ⊙ is the halo of electromagnetic origin; ● is the hadronic halo; ⊕ are the high energy hadrons; • are the family γ quanta; + are the hadrons of the family.

The parameter λ_m is the best known parameter of asymmetry describing the degree of alignment rather than the eccentricity. For example, λ_4 will be equal to 1 if four points belong to the same straight line, but it will be far less than 1 if these points form four vertices of a long rectangle.

V.V.Kopenkin, A.K.Managadze, I.V.Rakobolskaya, T.M.Roganova. Phys. Rev. **D 52**, 2776 (1995)

Alignment as a result of QCD jet production or of new still unknown physics at the LHC?

I.P. Lokhtin, A.K. Managadze, L.I. Sarycheva, A.M. Snigirev

Skobeltsyn Institute of Nuclear Physics, Moscow State University, 119992, Moscow, Russia

Eur. Phys. J. C 44, 51 (2005)
Yad. Fiz. 69, 117 (2006)

Abstract

The hypothesis of the relation between the apparent alignment of spots in the x-ray film reported from cosmic ray emulsion experiment and the features of events in which jet production prevails at super high energies is tested. Due to strong dynamical correlation between the jet axes and that between the momenta of jet particles (almost collinearity), the evalueted degree of aligment appears to be considerably larger than that for random selection of chaotic array of spots in the x-ray film. It is comparable with experimental data assuming that the height of primary interaction, the collision energy and the total energy of selected clusters meet certain conditions. The Monte Carlo generator PYTHIA, which basically well describes jet events in hadron-hadron interactions, was used for the analysis. New physical implications from the aligment phenomenon at the LHC are discussed. This talk is mainly based on our paper published in Eur. Phys. J. C44, 51-57 (2005).

The intriguing phenomenon: the strong collinearity of spot cores in emulsion experiments, closely related to coplanar scattering of secondary particles in the interaction, has been observed long time ago. So far there is *no simple satisfactory explanation of these cosmic ray observations in spite of numerous attempts to find it.*

In this respect, the jet-production mechanism looks very attractive as it offers a natural explanation of alignment of three spots along a straight line which results from momentum conservation for a simple parton picture of scattering.

Data from the Pamir Collaboration:

The families with the total energy of γ-quanta larger than a certain threshold and at least one hadron present were selected and analyzed. The alignment becomes apparent at

$$\Sigma E_\gamma > 0.5 \text{ PeV}.$$

The families are produced mostly by a proton with energy

$$\gtrsim 10 \text{ PeV}$$

interacting at the height h of several hundred metres to several kilometres in the atmosphere above the emulsion chamber.

The collision products are observed within a radial distance up to several centimetres in the emulsion where the spot separation is of the order of 1 mm.

We start from kinematics

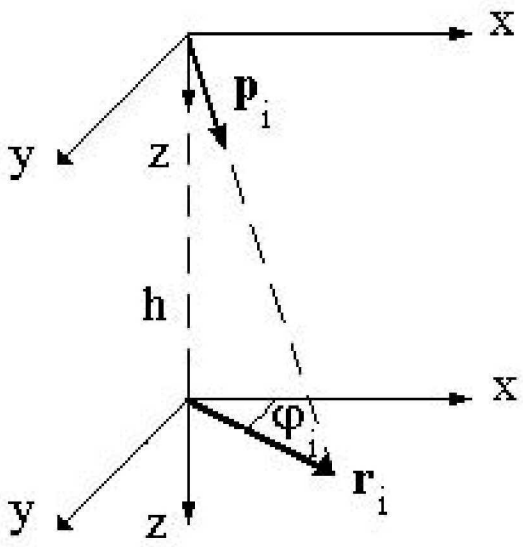

$\Leftarrow$ It is convenient to parametrize 4-momentum of each produced particle i using its transverse momentum p_{Ti} (relative to the collision axis z), azimuthal angle ϕ_i and rapidity η_i
in the center-of-mass system:

$$[\sqrt{p_{Ti}^2 + m_i^2}\ \cosh\eta_i,\quad p_{Ti}\cos\phi_i,\quad p_{Ti}\sin\phi_i,\quad \sqrt{p_{Ti}^2 + m_i^2}\ \sinh\eta_i].$$

If we neglect the subsequent interactions of particles penetrating through the atmosphere (this gives the maximum estimation of the alignment effect), then the position of each particle in the transverse (xy)-plane is easily calculated

$$\bar{r}_i \;=\; \frac{\bar{v}_{ri}}{v_{zi}}\, h \;=\; \frac{\bar{p}_{Ti}}{\sqrt{p_{Ti}^2 + m_i^2}\;\sinh(\eta_0 + \eta_i)}\, h \;,$$

where $\bar{v}_{ri}$ and v_{zi} are the radial and longitudinal components of particle velocity respectively;

$$E_i \;=\; \sqrt{p_{Ti}^2 + m_i^2}\;\cosh(\eta_0 + \eta_i)$$

is the particle energy in the laboratory frame and η_0 is the rapidity of the center-of-mass system in the laboratory frame.

Since the size of the observation region is of the order of several centimetres, these radial distances must obey the following restriction:

$$r_{\min} < r_i \qquad (1)$$

$$r_i < r_{\max} \qquad (2)$$

We set $r_{\min} = r_{\rm res} \simeq 1$ mm, $r_{\max} \simeq 15$ mm. The restriction (1) simply means that spots tested for alignment are not mixed with the central spot formed by the particles which fly close to the collision axis.

The separation of spots in the x-ray film gives another restriction on the distance between i-th and j-th particle

$$d_{ij} = \sqrt{r_i^2 + r_j^2 - 2r_i r_j \cos(\phi_i - \phi_j)}. \qquad (3)$$

It must be larger than 1 mm:

$$d_{ij} > r_{\rm res} , \qquad (4)$$

otherwise the particles must be combined in one particle-cluster until there remain only particles and/or particle-clusters with the mutual distances larger than $r_{\rm res}$, each such particle-cluster being considered as a single particle with coordinates defined in the same way as the center-of-mass coordinates of two bodies:

$$\bar{r}_{ij} = (\bar{r}_i E_i + \bar{r}_j E_j)/(E_i + E_j).$$

Then we select 2, ..., 7 clusters/particles which are most energetic and obey the restrictions (1, 2, 4), and calculate the alignment λ_{N_c} using the conventional definition:

$$\lambda_{N_c} = \frac{\sum\limits_{(i\neq j\neq k)}^{N_c} \cos(2\phi_{ijk})}{N_c(N_c-1)(N_c-2)},$$

and taking into account the central cluster, i.e. $N_c - 1 = 2, ..., 7$.

Here ϕ_{ijk} is the angle between two vectors $(\bar{r}_k - \bar{r}_j)$ and $(\bar{r}_k - \bar{r}_i)$ (for the central spot $\bar{r} = 0$).

The parameter λ_{N_c} characterizes the location of N_c points relative to a straight line and varies from $-1/(N_c-1)$ to 1.

For instance, in the case of symmetrical and close to most probable random configuration of three points in a plane (the equilateral triangle)

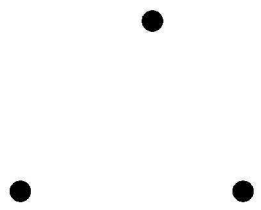

$$\lambda_3 = -0.5.$$

The ultimate case of perfect alignment corresponds to $\lambda_{N_c} = 1$ when all points lie exactly along the straight line (• • . . . • • •),

while for an isotropic distribution $\lambda_{N_c} < 0$.

The alignment degree P_{N_c} is defined as a fraction of events with

$$\lambda_{N_c} > 0.8$$

with the number of spots not less than N_c.

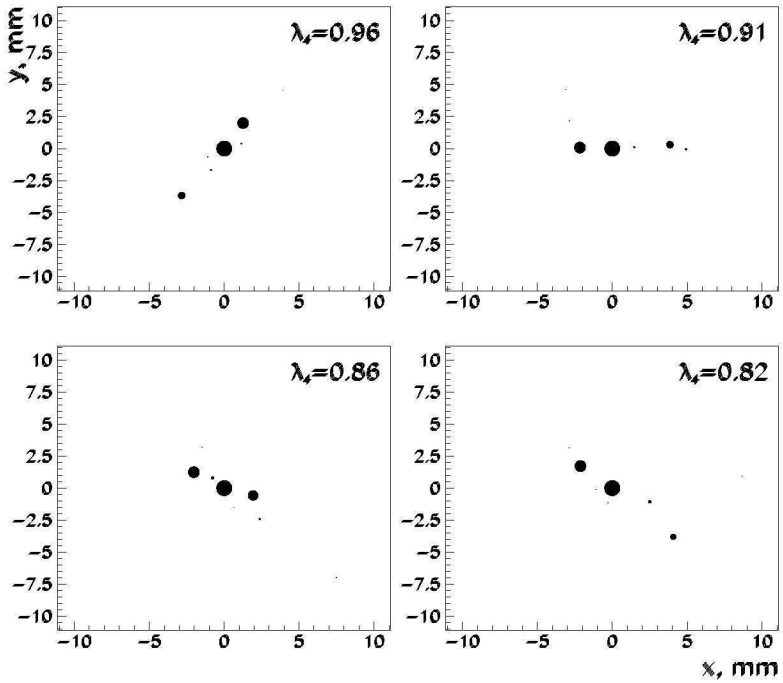

⇐ Samples of spot core distributions for simulated events with $E_\Sigma^{\rm thr} = 10\,{\rm PeV}$ and $\lambda_4 > 0.8$. The size of spots is proportional to their energy (except for the central spot which is not to scale).

If the hypothesis about the relation of alignment to the prevailing jet character of events at super high energies is valid, then this effect must manifest itself first of all in nucleon-nucleon collisions.

Therefore, to be specific we consider a collision of two protons and fix the primary energy in the laboratory system $E_{\rm lab} \simeq 9.8 \times 10$ PeV, that is equivalent to $\sqrt{s} \simeq 14$ TeV — just the LHC energy (the rapidity shift being $\eta_0 \simeq 9.55$ after the transformation from the center-of-mass to the laboratory system).

To simulate a collision of two protons with such energies we use the Monte Carlo generator PYTHIA, which basically well describes jet events in hadron-hadron interactions and is tuned using the available data from accelerator experiments.

We set the following parameters:

$$r_{\min} = r_{\rm res} = 1 \text{ mm}, \; r_{\max} = 15 \text{ mm}, \; h = 1000 \text{ m},$$

with the additional restriction on the energy threshold for particle registration in the emulsion:

$$E_i > E^{\rm thr} = 4 \text{ TeV}.$$

This is close to the conditions of emulsion experiments.

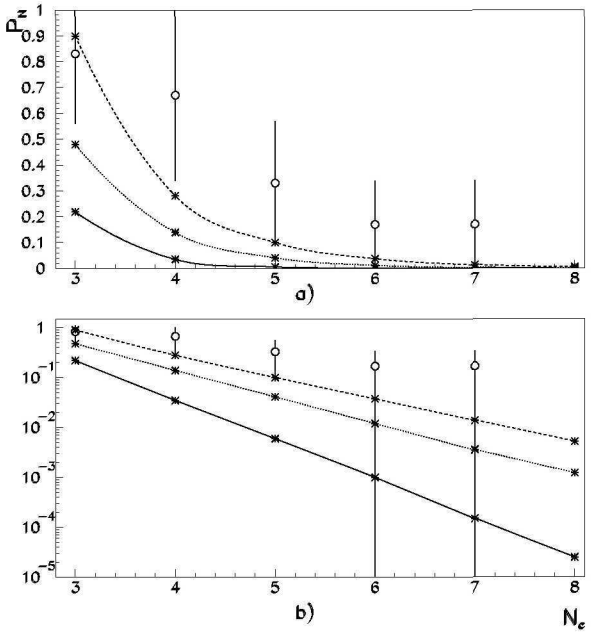

⇐ The alignment degree P_{N_c} as a function of cluster number N_c at $h = 50$ m and $\sqrt{s} = 14$ TeV on linear (a) and logarithmic (b) scale. The solid curve coresponds to $h = 1000$ m without restriction on the minimum value of process hardness $p_T^{\rm hard}$, the dotted curve — $p_T^{\rm hard} = 300$ GeV, the dashed curve — $p_T^{\rm hard} = 3$ TeV. Points (○) with errors are experimental data.

The estimated degree of alignment P_{N_c} for N_c spot cores is considerably larger than that for random selection of chaotic array of spots in the x-ray film, but is still too small (by a factor of 3—4) to describe the experimental data even taking into account large experimental errors.

WHY???

Let us consider the effect of the applied restrictions (1, 2) (the laboratory acceptance criterion) on the spectrum of particles selected to calculate the alignment.

For particles with high enough transverse momentum p_{Ti} relative to the mass m_i these conditions (1, 2) are reduced mainly to the restriction on the available particle rapidities in the center-of-mass system:

$$r_{\min} < r_i \Longrightarrow \eta_i < \eta_{\max} = \ln(r_0/r_{\min}) \simeq 4.95, \qquad (5)$$

$$r_i < r_{\max} \Longrightarrow \eta_i > \eta_{\min} = \ln(r_0/r_{\max}) \simeq 2.25, \qquad (6)$$

since in this case $r_i \simeq r_0/e^{\eta_i}$ for $\eta_0 + \eta_i \gtrsim 1$, where

$$r_0 = 2h/e^{\eta_o}. \qquad (7)$$

Thus, detected in the x-ray film are the ultrarelativistic particles $(p_{Ti} \gg m_i)$ from the restricted rapidity region (see eqs. 5, 6 bellow) which excludes such configurations as back-to-back hard jets with rapidities close to zero in the center-of-mass system:

$$r_{\min} < r_i \Longrightarrow \eta_i < \eta_{\max} = \ln(r_0/r_{\min}) \simeq 4.95, \qquad (5)$$

$$r_i < r_{\max} \Longrightarrow \eta_i > \eta_{\min} = \ln(r_0/r_{\max}) \simeq 2.25, \qquad (6)$$

since in this case $r_i \simeq r_0/e^{\eta_i}$ for $\eta_0 + \eta_i \gtrsim 1$, where $r_0 = 2h/e^{\eta_o}$. The configurations with scattering of hard partons at angles close to 90° in the considered hadronic center-of-mass system (which in this case practically coincides with the partonic center-of-mass system) can be expected to be responsible for the alignment phenomenon.

Ultrarelativistic particles from the central rapidity region in the hadron center-of-mass system (as possible sources of appropriately correlated spots) can get into the observation region because of decrease of r_0 *only*, i.e. the decrease of the height h of primary interaction or the increase of the rapidity η_0 of the center-of-mass system due to the growth of energy $\sqrt{s}$, as it follows from (7).

For illustration we use the first, or "less dangerous" alternative — decrease of the interaction height by a factor of 20 rather than increase of the energy $\sqrt{s}$ by the same factor of 20 at the same height so that particles from both hard jets (with back-to-back structure), hitting the registration plane, come from some rapidity range near $\eta_i \simeq 0$ including adjucent positive and negative values.

In this case the alignment degree becomes strongly dependent on the minimum transverse momentum of hard process, $p_T^{\rm hard}$, which is a parameter of PYTHIA. At the height $h = 1$ km such dependence is not visible, although we might catch some marginal tendency of the alignment degree to grow with the increase of $p_T^{\rm hard}$ at such height. However without the restriction on $p_T^{\rm hard}$ from below (minimum bias) the result coincides practically with that obtained earlier (solid curve in previous Fig.)

If $p_T^{\rm jet} \geq 3$ TeV, particles from these hard jets together with particles flying close to z-axis (within the transverse radius < 1 mm) result in the alignment degree (dashed curve) COMPARABLE with the experimentally observed one.

Thus the jet-production mechanism can, in principle, explain the results of emulsion experiments. For such an explanation it is necessary (but not sufficient) that particles from both hard jets (with rapidities near $\eta_i \simeq 0$ in the center-of-mass system) get into the observation region.

This is possible:

at the relatively small height $h = 50$ m and $\sqrt{s} \simeq 14$ TeV; or
at $h = 1000$ m, yet considerably higher $\sqrt{s} \simeq 14 \times 20 = 280$ TeV; or
at some reasonable intermediate combination of h, $\sqrt{s}$, $r_{\max}$ which meets the following condition:

$$r_0 = 2h/e^{\eta_0} = 2hm_p/\sqrt{s} \lesssim kr_{\max}, \qquad (8)$$

where m_p is the proton mass. $k \simeq 1/2 < 1$ is needed to have particles with $\eta_i < 0$ getting into the detection region.

We verified the decisive significance of condition (8) to allow observation of high-degree alignment and its dependence on the process hardness for the lower energy $\sqrt{s} \simeq 1.4$ TeV (where the prediction of PYTHIA is quite adequate) and the height $h = 5$ m (in accordance with (8)), thereby confirming such a peculiar kinematic "scaling".
At $p_T^{\rm hard} = 3$ TeV jets carry away about half of the energy of colliding protons in the center-of-mass system $\xi \simeq 2p_T^{\rm jet}/\sqrt{s}$, where ξ is a fraction of proton energy carried by each interacting parton (quark or gluon).

The striking feature of such configurations in the x-ray film is approximate equality of energy deposition in the central and the rest most energetic clusters, that can be used to select the events with very hard jets, and not only at the generator level (simulation).

Introduction of another threshold on the total energy of all the $(N_c - 1)$ selected clusters $E_\Sigma^{\rm thr} \sim E_{\rm lab}/2$ (without taking into account the energy deposition in the central cluster $r = 0$),

$$\sum_{l=1}^{N_c-1} E_l > E_\Sigma^{\rm thr},$$

allows us to select the events with hard jets only in a "natural" physical way and reduce the hypothesis to the physically acting mechanism.

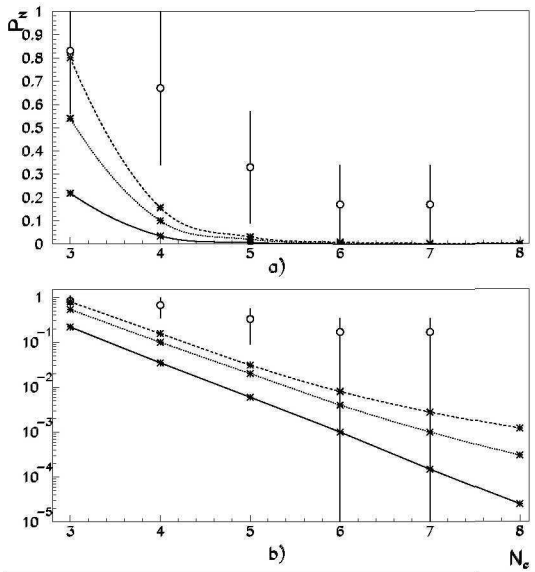

$\Leftarrow$ The alignment degree P_{N_c} as a function of cluster number N_c at $h = 50$ m and $\sqrt{s} = 14$ TeV on linear (a) and logarithmic (b) scale. The solid curve corresponds to $h = 1000$ m without restriction on the total cluster energy $E_\Sigma^{\rm thr}$, the dotted curve — $E_\Sigma^{\rm thr} = 2$ PeV, the dashed curve — $E_\Sigma^{\rm thr} = 10$ PeV. Points (○) with errors are experimental data.

We see that the alignment increases with the growth of $E_\Sigma^{\rm thr}$ (the restriction on $p_T^{\rm hard}$ is absent at all!), and it becomes large enough (dashed curve) and COMPARABLE with the experimentally observed one above the threshold $E_\Sigma^{\rm thr} \simeq 0.1 E_{\rm lab} \simeq 10$ PeV.

One should note, though, that our estimations give still too steep dependence of P on N_c as one can see from a comparison of the slopes of the straight lines with the behaviour of experimental points.

Besides, for jet events

$$\frac{P_{N_c}}{P_{N_c+1}} = \text{const}$$

with high accuracy

To give one a feeling of various measures of alignment we present here the spatial distributions of the most energetic clusters in the (xy)-plane for a few generated events, and the corresponding values of λ_{N_c}.

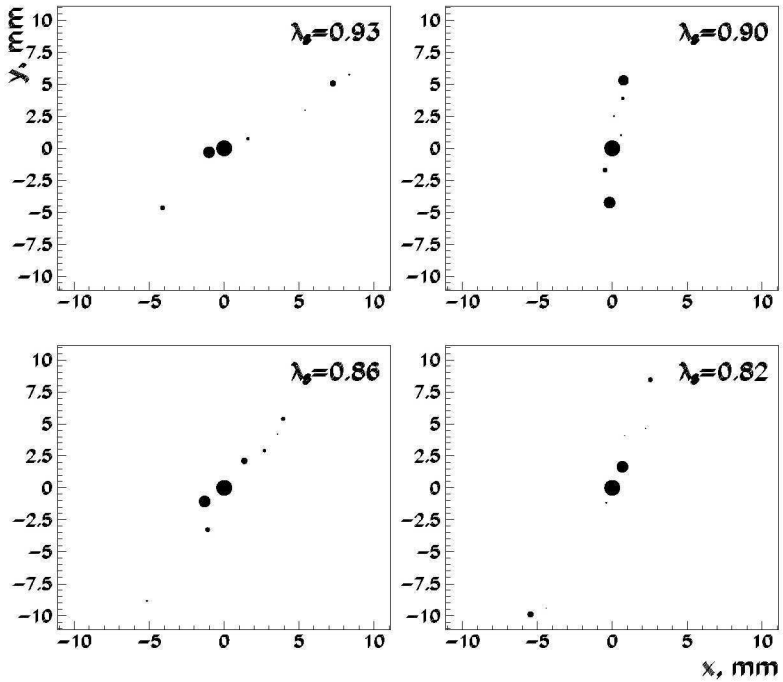

$\Leftarrow$ Samples of spot core distributions for simulated events with $E_\Sigma^{\rm thr} = 10\,{\rm PeV}$ and $\lambda_8 > 0.8$. The size of spot is proportional to its energy (except for the central spot which is not to scale).

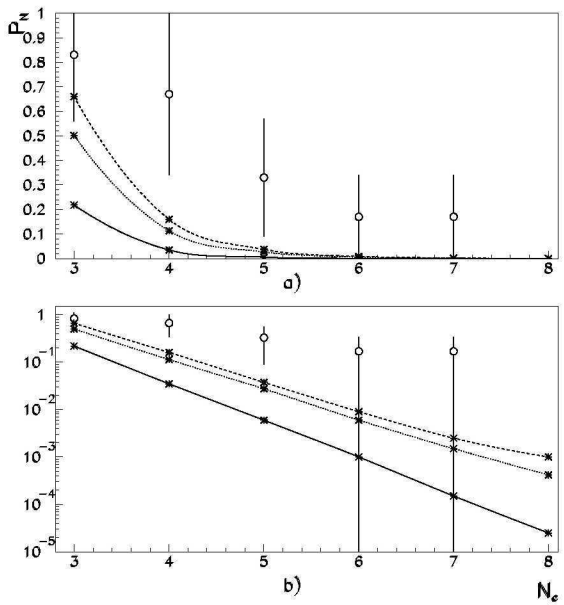

⇐ The alignment degree P_{N_c} as a function of cluster number N_c at $h = 50$ m and $\sqrt{s} = 14$ TeV on linear (a) and logarithmic (b) scale. The solid curve corresponds to $h = 1000$ m without restriction on the total energy $E_\gamma^{\rm thr}$ of γ-quanta, the dotted curve — $E_\gamma^{\rm thr} = 1$ PeV the dashed curve — $E_\gamma^{\rm thr} = 5$ PeV. Points (o) with errors are experimental data.

If the jet-production mechanism alone is insufficient to describe the observed alignment and there are another mechanisms of this effect at the energy $\sqrt{s} \sim 14$ TeV and the height $h \sim 1000$ m (mostly used in emulsion experiment estimations), then in any case some sort of alignment should *arise* at LHC *too* in the rapidity region (defined by eqs. 5, 6).

This region must be investigated more carefully on the purpose to study the azimuthal anisotropy of energy flux in accordance with the procedure applied in the emulsion and other experiments, i.e. one should analyze the energy deposition in the cells of $\eta \times \phi$-space in the rapidity interval (5, 6) (the equivalent threshold minimum particle energy being $E^{\rm thr}_{\rm c.m.s.} = E^{\rm thr}/\cosh\eta_0 \simeq 2E^{\rm thr}/e^{\eta_0} \simeq 0.6$ GeV in the center-of-mass system).

Note that the absolute rapidity interval can be shifted: it is only necessary that the difference $(\eta_{\rm max} - \eta_{\rm min})$ be equal to $\simeq 2.7$ in accordance with the variation of radial distance by a factor of 15 $(r_{\rm max}/r_{\rm min} = 15)$ due to the relationship $r_i \simeq r_0/e^{\eta_i}$ (independent on r_0).

Conclusions

- Our analysis shows that for pp-collision at a fixed height of primary interaction of the energy $\sqrt{s}$, when the condition (8) works — that is, ultrarelativistic particles from the rapidity interval near $\eta_i \simeq 0$ in the center-of-mass system fall into the observation region inside the radius $r_{\max}$ in the laboratory frame due to large Lorentz factor — *an alignment of spots arises* and the alignment degree becomes strongly dependent on the process hardness. This, in principle, explains the existence of the experimental energy threshold of this effect.

- Introducing another additional threshold (the scale of which is determined by the energy of an incident proton) on the total energy of all the $(N_c - 1)$ selected most energetic clusters (without taking into account the energy deposition in the central cluster) allows us to select the events with high hardness in a "natural" physical way and thereby support the jet-production hypothesis.

- Meanwhile we suggest a more careful investigation of the rapidity region (defined by eqs. 5, 6) at LHC in order to reveal the NEW still UNKNOWN mechanisms of alignment if those exist.

Acknowledgements. It is a pleasure to thank A.I.Demianov, S.V.Molodtsov, V.I.Osedlo, S.A.Slavatinsky, L.G.Sveshnikova, K.Yu.Teplov and G.T.Zatsepin for discussions.

References

1. Pamir Collaboration, in Proc. of the 21st Int. Cosmic Ray Conf., Adelaide, Australia (1989), edited by R.J.Protheroe (University of Adelaide, Australia), 227 (1990); S.A.Slavatinsky, in Proc. of the 5th Int. Symp. on Very High Energy Cosmic Ray Interactions, Lodz, Poland (1988), edited by M.Giler (University of Lodz, Lodz, Poland), 90 (1989)
2. V.V.Kopenkin et al. Phys. Rev. D 52, 2766 (1995)
3. F.Halzen, D.A.Morris, Phys. Rev. D 42, 1435 (1990)
4. T.Sjostrand, Comp. Phys. Com. 135, 238 (2001)
5. I.V.Rakobolskaya et al., The peculiarity of hadron interactions of cosmic rays at super-high energies (MSU, Moscow 2000) (in Russian)
6. Yu.L.Dokshitzer et al., Phys. Rep. 58, 269 (1980)
7. V.V.Kopenkin en al., Izv. Rus. Akad. Nauk. Ser. Fiz. 58, 13 (1994)
8. D.Cline et al., Phys. Rev. Lett. 31, 491 (1973)
9. Z.Cao et al., Phys. Rev. Lett.. 72, 1794 (1994)
10. Z.Cao et al., Phys. Rev. D56, 7361 (1997)
11. V.N.Gribov, L.N.Lipatov, Sov. J. Nucl. Phys. 15, 438, 675 (1972)
12. L.N.Lipatov, Sov. J. Nucl. Phys. 20, 94 (1974)
13. Yu.L.Dokshitzer. Sov. J. JETP 46, 641 (1977)
14. G.Altarelli, G.Parisi, Nucl. Phys. B 126, 298 (1977)
15. I.P.Lokhtin et al., Eur. Phys. J. C 44, 51 (2005)
16. I.P.Lokhtin et al., Yad. Fiz. 69, 117 (2006) (in Russian)

Appendix

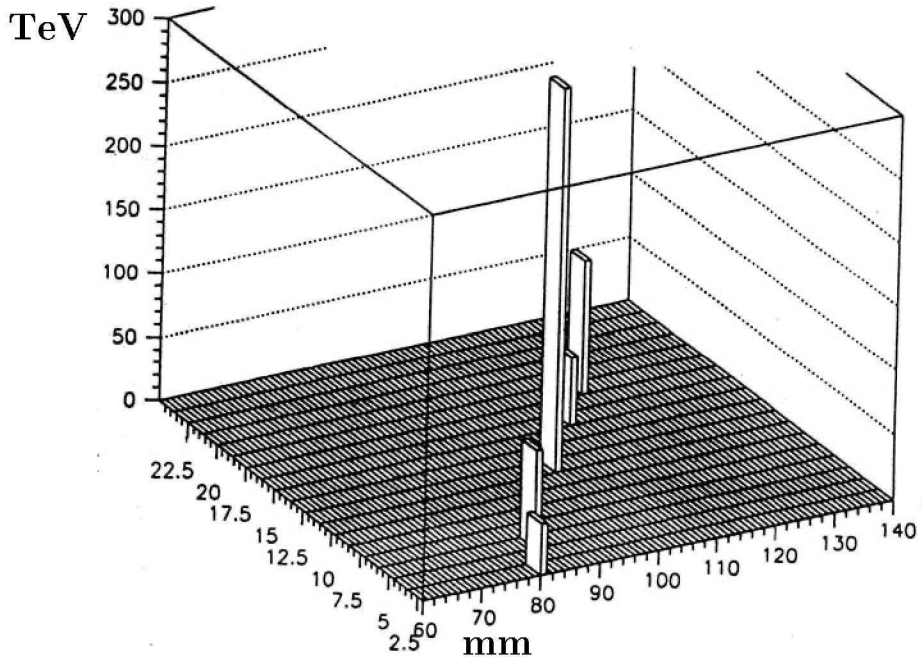

Family of γ-quanta with the energies $E_\gamma > 50$ TeV (experiment "Concord", H = 17 km). $\sum E_\gamma \approx 1600$ TeV, $E_0 = 10^{16}$ eV. Aligned are 38 particles of 211.

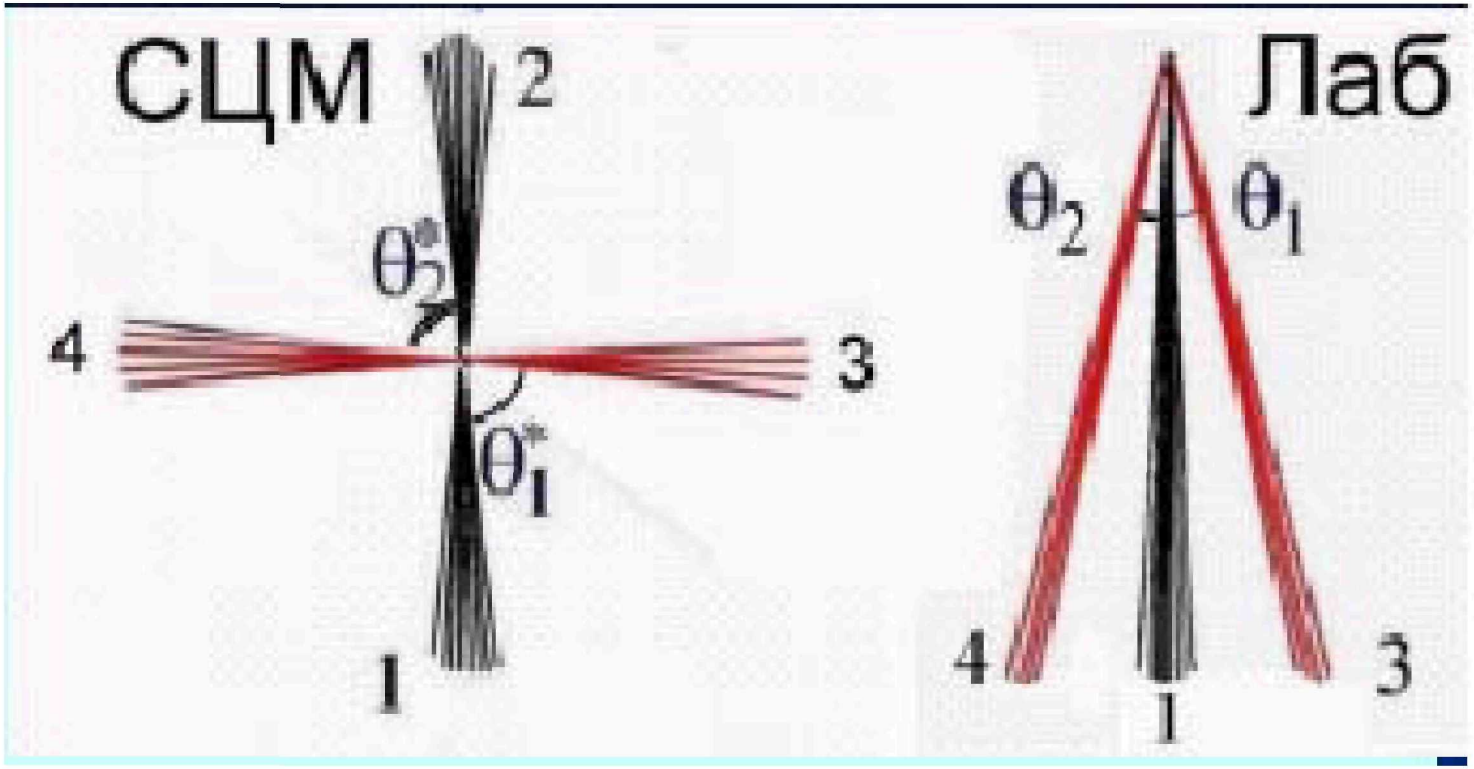

Illustration of jet mechanism generating the alignment due to center-of-mass to laboratory transformation.

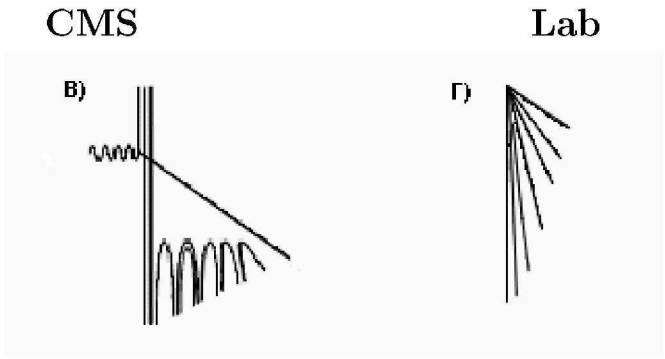

The alignment due to break of qg-string.

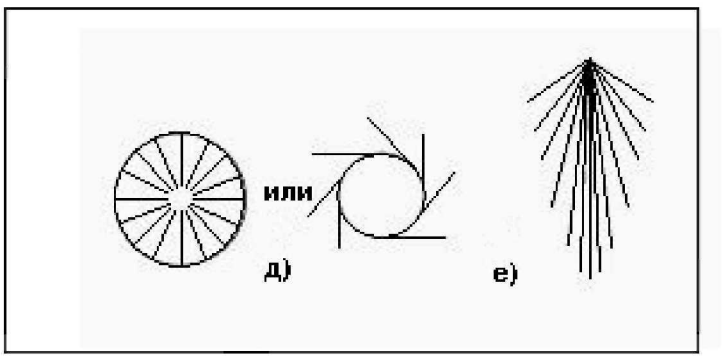

The alignment due to rotation of "bag quarks".

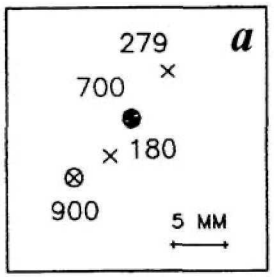

$\lambda_4 = 0.91$

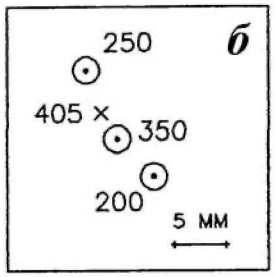

$\lambda_4 = 0.85$

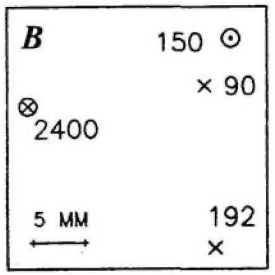

$\lambda_4 = 0.22$

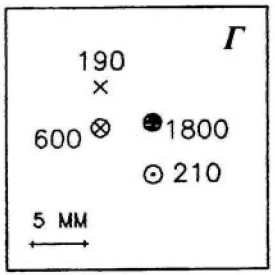

$\lambda_4 = 0.12$

Experiment "Pamir"(H = 4370 m), roentgen-emulsion chamber.

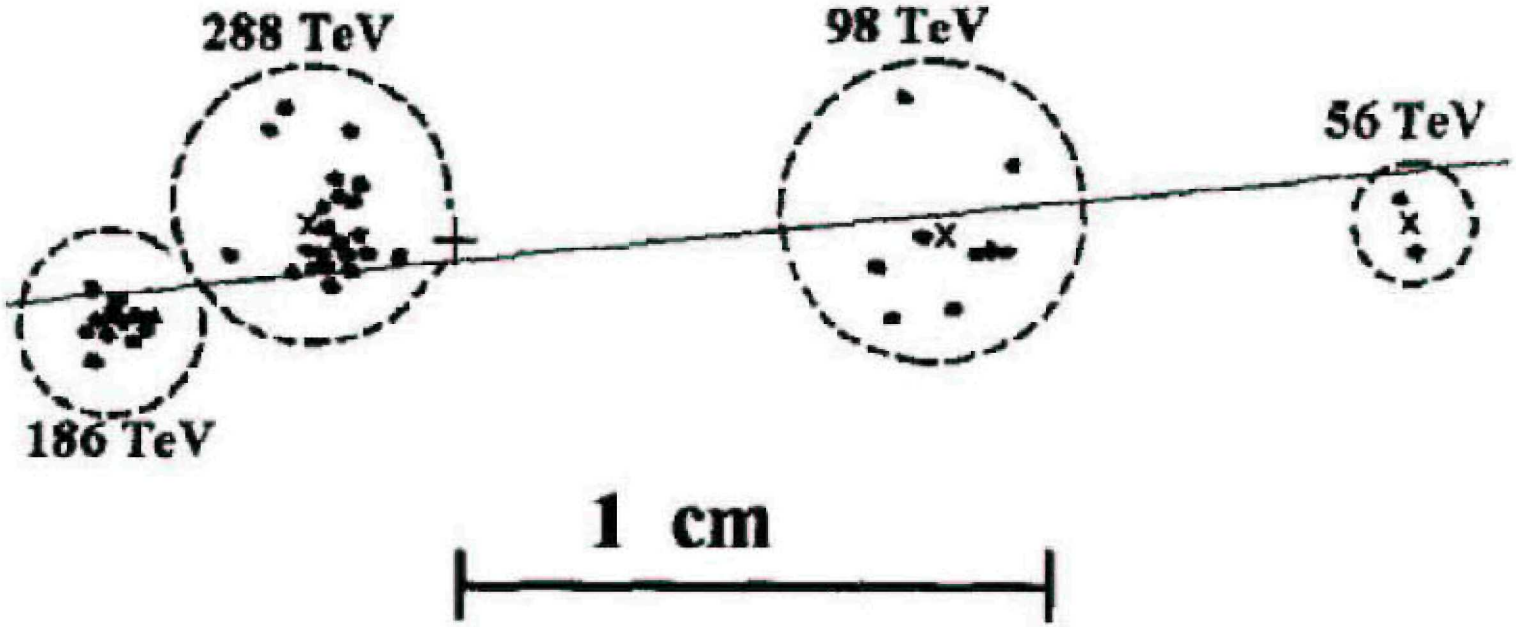

A sample of γ-family in C-chambers with aligned γ-clusters (experiment "Pamir").

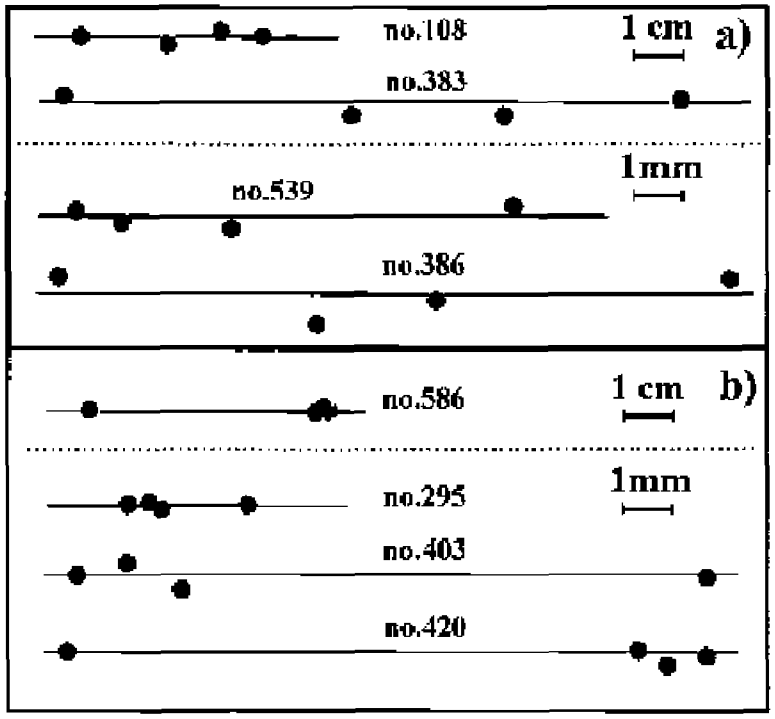

Experimental target diagrams with aligned clusters in C-chambers (numbers are refer to particular families).

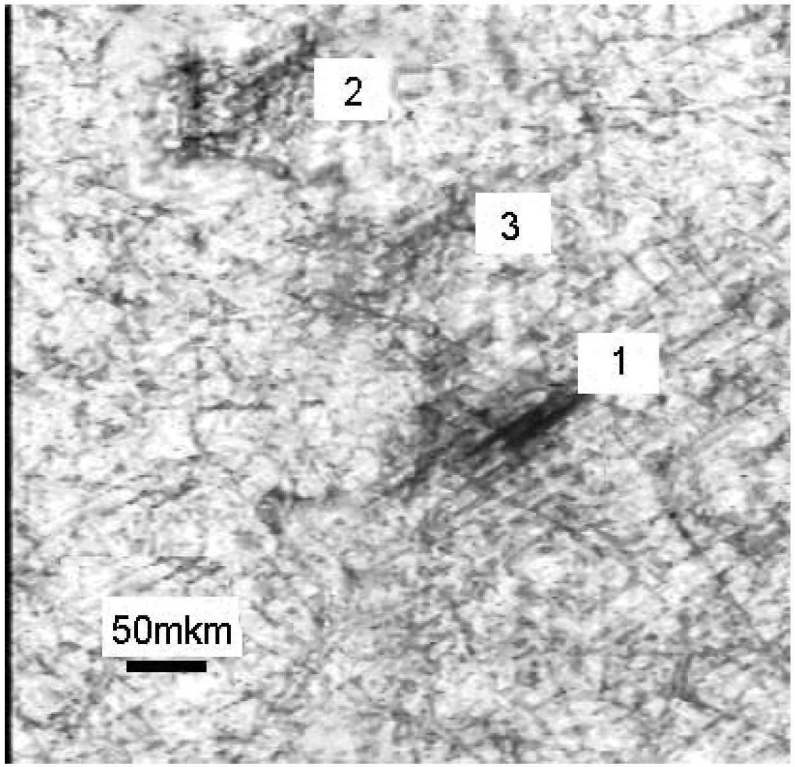

A sample of aligned tracks in nuclear emulsion from the database RUNJOB. (Flight altitude H≈ 17 km).

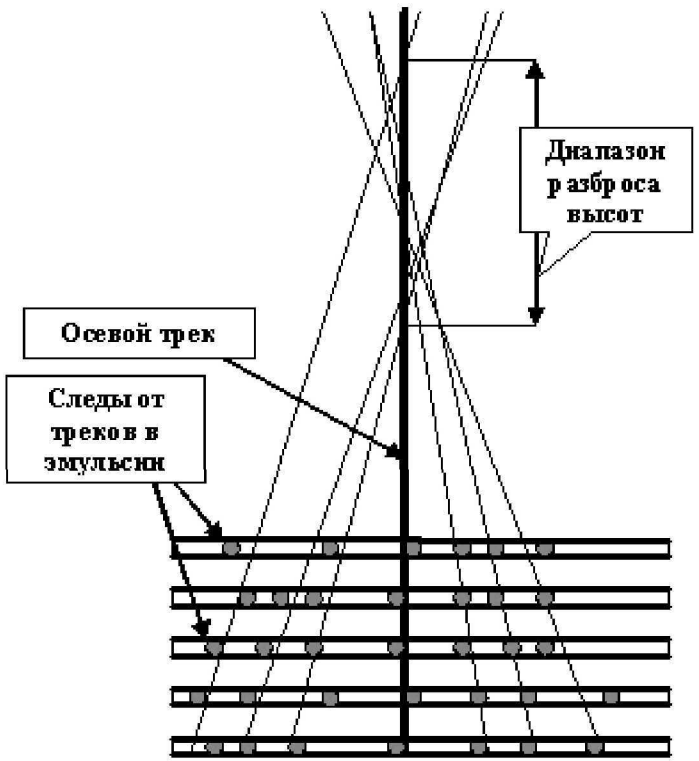

Triangulation diagram for vertex height evaluation about the chamber stack. Super-family "STRANA", $E_0 \sim 10^{16}$ eV. (Flight altitude H$\approx$ 17 km).

2. High energy Cherenkov gluons at RHIC and LHC

Cherenkov photons and Mach shock waves are wellknown collective effects in physics. Both have the similar origin-wave radiation by a body moving with speed exceeding the wave velocity c_w, i.e. the phase velocity. If z-axis is chosen along the body propagation, then in both cases emission in an infinite medium at rest is directed along the cone with the polar alnge θ defined by the condition

$$\cos\theta = \frac{c_w}{v}. \tag{1}$$

For Cherenkov photons $c_w = c/n$ where n is the index of refraction, for Mach waves $c_w = c_s$ where c_s is the sound velocity in the medium.

Are there analogues of these effects for strong interactions?

The intuitive picture which comes to mind is to consider the impinging partner in hh, hA, AA collisions as a bunch of partons passing through a hadronic medium. A target hadron or nucleus can be treated as a nuclear slab with a definite index of *nuclear* reaction. The analogue to Cherenkov photons would be Cherenkov gluons emitted by a parton entering this hadronic medium.

There are some indications from experiment on coherent collective effects in hadronic matter which result in the so-colled ring-like events.

The main experimental signature of both effects would be two peaks in the pseudorapidity distribution of particles produced in high energy nuclear collisions which are positioned in accordance with Eq. (1). The most visual image of these effects is the ring-like structure of events in the plane perpendicular to the direction of propagation of the body initiating them.

For gluons, $c_w = c/n$ where n is their nuclear index of refraction in a nuclear matter through which they move. The necessary condition for this effect is that the real part of the index of refraction be larger than 1. This index was estimated from experimental data on hadronic ractions with assumption that gluons as carriers of strong forces should possess the features common to hadronic reactions.

The real part of the nuclear index of refraction can be written as

$$\mathrm{Re}n^r = 1 + \Delta n_R^r = 1 + \frac{3m_\pi^3}{2\omega_r^2\Gamma}. \tag{2}$$

Here ω_r is the energy required to produce a resonance. It can be of the order of the pion mass m_π. Since the widths of known resonances Γ are of the order of hundred MeV, Δn_R^r can be of the order of 1. Therefore, according to (1), the angle of particles emission is rather large in the target rest system. The effect can be observed at RHIC and LHC if initial partons (jets) move at a large angle with respect to the collision axis. In such a way one can try to interpret the recently observed at RHIC effect with two peaks in angular distribution about the direction of propagation of the companion jet created in the direction perpendicular to the collision axis. The peak position showed that $c_w = 0.33c$. Thus, it could be the emission of low energy Cherenkov gluons with nuclear index of refraction equal to 3.

2. High energy Cherenkov gluons at RHIC and LHC

In what follows we discuss high energy Cherenkov gluons at RHIC and LHC energies produced by forward moving partons. The important problem of experimental search for this effect is the shape of the background due to "ordinary" processes.

To estimate the background we have used the HIJING model for central collisions ($b = 0$) for Au-Au collisions at RHIC energy $\sqrt{s} = 200A$ GeV and for Pb-Pb collisions at LHC energy $\sqrt{s} = 5500A$ GeV. 3500 events were generated in each case.

Then the pikes in individual HIJING events exceeding the regular distribution by more than one and two standard deviations have been separated. They can appear either as purely statistical fluctuations or as hard QCD-jets. FIGs 1a and 2a show the examples of such events (for RHIC and LHC energies, correspondingly) plotted over the smooth inclusive pseudorapidity distributions.

FIGs 1b and 2b show these distributions for peaks exceeding the inclusive background at RHIC and LHC energies by two or one standard deviations. It is seen that these distributions are flat with extremely small irregularities. This agrees with our expectations that statistical fluctuations and QCD jets do not have any preferred emission angle and should be randomly dispersed over the inclusive particle distribution. They can be considered as background for experimental search for Cherenkov gluons which do have such preferred angle. High energy Cherenkov jets should have quite narrow angular spread. If their angular width corresponds to a single bin in FIGs 1 and 2, then they would produce peaks twice exceeding this background even when their cross section is only 5 per cent of the cross section in the considered interval of pseudorapidities. If experimental data on group centers distribution show some peaks at definite pseudorapidity values over this background, this can be indicative of new collective effect, not considered in HIJING. These finding may be added to the experimental evidence in favor of such effect collected before.

It is easy to check from FIGs that the levels of the background for 1σ and 2σ fluctuations correspond to the traditional statistical estimates of about 30% and 5%.

To conclude, the pseudorapidity distributions of the centers of dense isolated groups of particles (jets) exceeding in individual events the inclusive distribution are plotted for events generated according to HIJING model at RHIC and LHC energies. They are very flat and provide the background for further searches for such collective effects as Cherenkkov gluons and Mach waves. If the peaks in the pseudorapidity plot of the centers of separated groups are found in experiment and fit the condition (1), then it will testify in favor of a Cherenkov gluons hypothesis. The positions of the peaks reveal such property of hadronic matter as its nuclear index of refraction and can be valuable for understanding the equation of state of the nuclear medium.

This work was presented at "Quark Matter'2005".

2. High energy Cherenkov gluons at RHIC and LHC

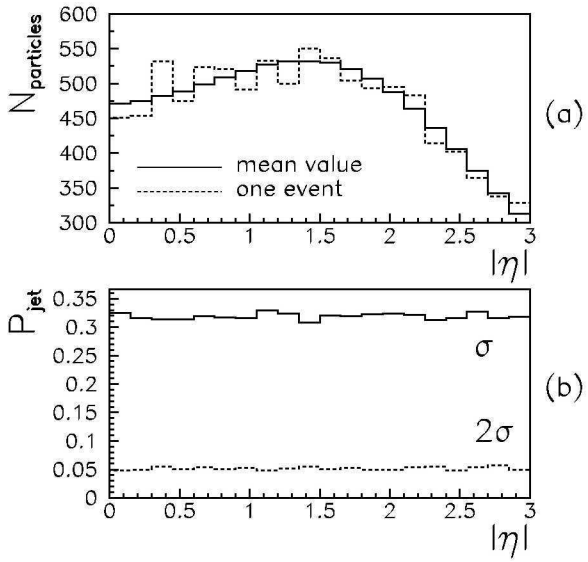

FIG. 1. (a) The pseudorapidity distribution in one of HIJING events (dashed histogram) for central Au-Au collision at $\sqrt{s} = 200A$ GeV is plotted over the inclusive HIJING distribution (solid histogram), $N_{\rm particles}$ — number of particles. Peaks above the inclusive plot are clearly seen. (b) The pseudorapidity distribution of the centers of dense isolated groups of particles similar to those shown in FIG. 1a and exceeding the inclusive plot by two and one standard deviations σ, $P_{\rm jet}$ — probability to find peak above mean $+\sigma(2\sigma)$. This is the smooth background for further searches of collective effects.

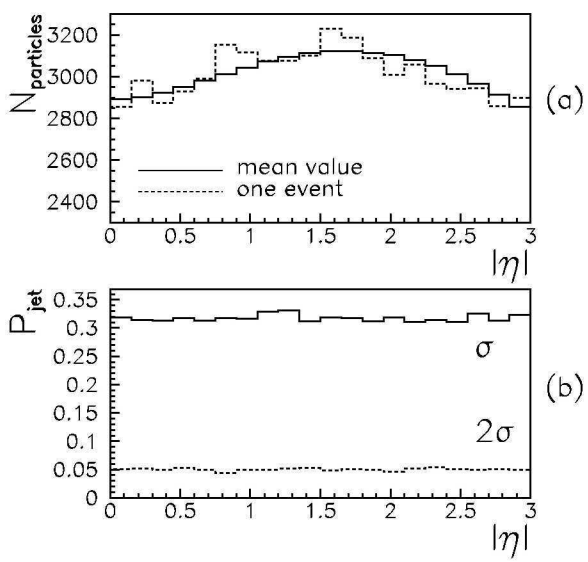

FIG. 2. (a) The pseudorapidity distribution in one of HIJING events (dashed histogram) for central Pb-Pb collision at $\sqrt{s} = 5500A$ GeV is plotted over the inclusive HIJING distribution (solid histogram), $N_{\rm particles}$ — number of particles. Peaks above the inclusive plot are clearly seen. (b) The pseudorapidity distribution of the centers of dense isolated groups of particles similar to those shown in FIG. 2a and exceeding the inclusive plot by two and one standard deviations σ, $P_{\rm jet}$ — probability to find peak above mean $+\sigma(2\sigma)$. This is the smooth background for further searches of collective effects.

I.M.Dremin. Ring-like events: Cherenkov gluons or Mach waves?
I.M.Dremin, L.I.Sarycheva, K.Yu.Teplov. High energy Cherenkov gluons at RHIC and LHC.

3. Possibility of Observing CENTAURO Events with HF Calorimeter of the CMS Detector

As the wide spectrum of exotic events seen in cosmic ray experiments is observed at *forward rapidities*, thus this region seems to be a potential place for the new physics. Unfortunately, the physics in the very forward rapidity region in ultra-relativistic nucleus-nucleus collisions has not been rigorously addrssed by theory so far. The main reason is the difficulty of the calculations in an enviroment of finite baryochemical potential. There are, however, some phenomenological and QCD-inspired attempts to predict new phenomena or to explain unusual phenomena already seen. It is expected that this region will contain only a small fraction of the totally produced particles and at the same time the vast majority of the available total energy with the baryon density reaching here the maximum. FIG. 1 shows the pseudorapidity distributions of multiplicity and energy, obtained in simulations (HIJING henerator) of 50 central Pb+Pb collisions at LHC energies $\sqrt{s} = 5.5$ TeV).

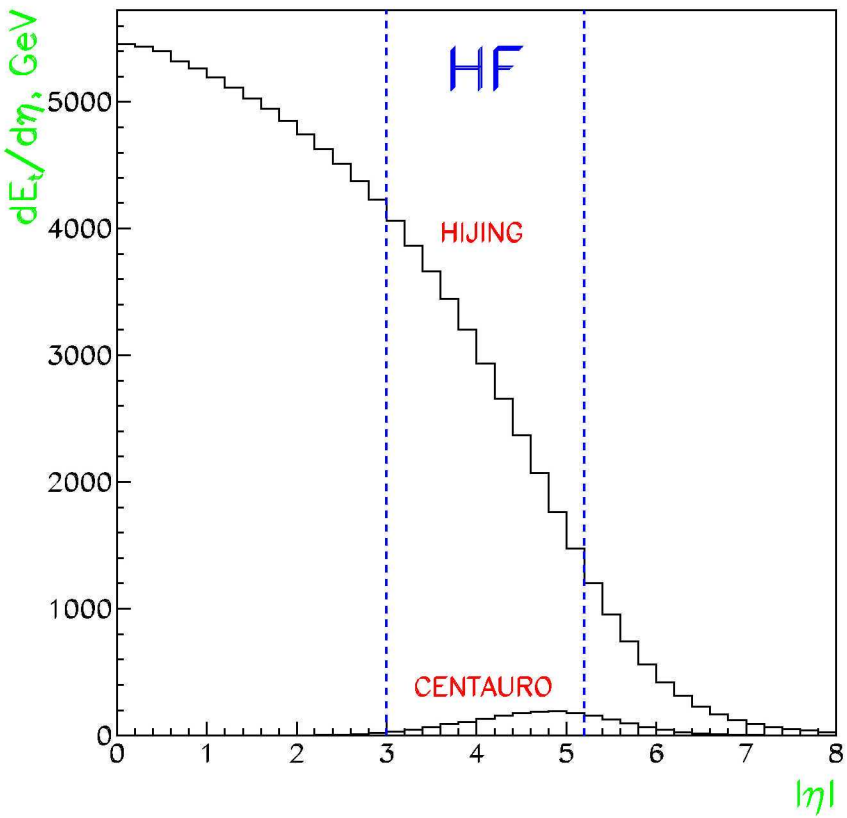

FIG. 1. Pseudorapidity distribution for Pb-Pb collisions for $b = 0$ and energy $5.5A$ TeV.

I.P.Lokhtin, S.V.Petrushanko, L.I.Sarycheva. SINP MSU

3. Possibility of Observing CENTAURO Events with HF Calorimeter of the CMS Detector

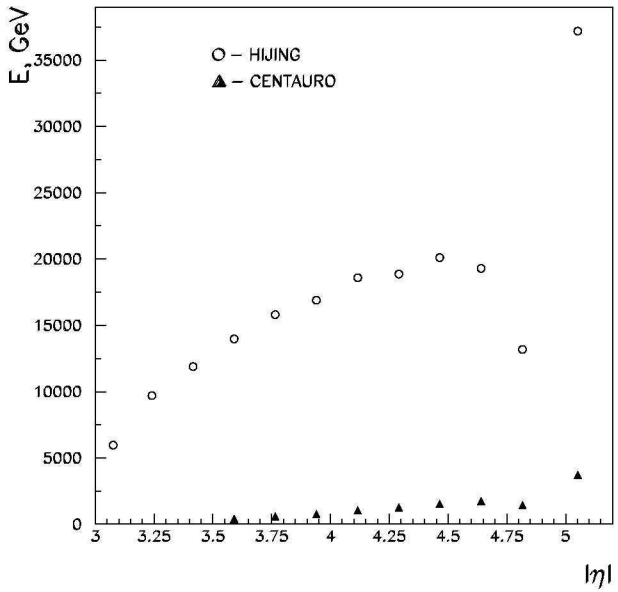

FIG. 2. Total energy responses in HF-calorimeter for HIJING and CENTAURO events.

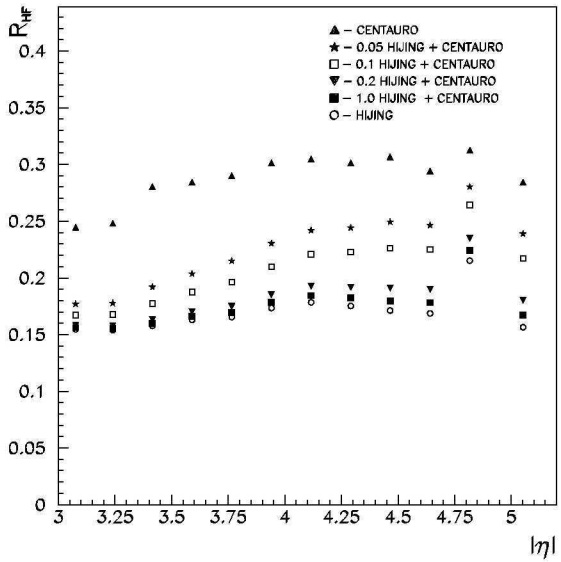

FIG. 3. R_{HF} for CENTAURO, HIJING and HIJING+CENTAURO.

- **CENTAURO — fireball**
  The Monte-Carlo code CNGEN v.1.13
  (Centauro Event Generator)
- HIJING v.1.34 model
  central Pb-Pb collisions:
  impact parameter $b = 0$ fm, $\sqrt{s} = 5.5$ GeV/n

CMSIM 125 — to get CMS detector responses

The phenomenological model is formolated in terms of impact parameter b of the ion collisions, two thermodynamical parameters, baryochemical potential μ_b and temperature T, and the nuclear stopping power Δy_{stop}.
According to the model the Centauro events occur in the projectile fragmentation region when the projectile nucleus penetrating through the target nucleus transforms its kinetic energy into heat and forms got quark matter (Centauro fireball) with high baryochemical potential.

I.P.Lokhtin, S.V.Petrushanko, L.I.Sarycheva. SINP MSU

4. Strangelets and QGP

The Exotic Features of Hadronic Cascade Fluctuations in an Ionization Calorimeter

A.I.Demianov, V.S.Murzin, L.I.Sarycheva
Institute of Nuclear Physics, Moscow State University, Moscow, Russia

Abstract

Studies on the hadronic cascade fluctuations, performed in cosmic rays using the ionization calorimeter, are indicative of a new mechanism of hadron-nucleus interaction that may appear at high energies — the mechanism which creates massive (~ 10 GeV/c^2) stable ($\gtrsim 10^{-11}$sec) particles with interaction length in a dense absorber substantially longer than that of nucleons.

Existence of such kind mechanism provides a reasonable explanation for the number of "exotic" phenomena, reported by different authors from different experiments, and is significant in that it points toward the type of effects to be expected from a change in the characteristics of interaction at high energies.

Introduction

The total absorption principle for measurement of elementary particle energy was known long ago. Apparently, the earliest successful implementation of this principle in order to measure the energy of electrons and photons in accelerator experiment dates back to 1954 [1]). The first total absorption spectrometer for measuring the energy of cosmic ray hadrons was constructed in 1957 [2]). Many a theoretical and experimental studies of the calorimeter properties, and numerous accelerator and cosmic ray experiments based on the calorimeter technique performed later on, considered the calorimeter mainly as a device measuring the *total* energy of incident electrons, photons and hadrons [3,4,5,6]). Meanwhile, the (sampling) ionization calorimeter with sufficiently fine longitudinal and transverse segmentation in itself makes it possible to trace the *dynamics* of nuclear cascade development in a dense medium and thereby investigate various characteristics of the processes of multiparticle hadroproduction on nuclei at high energies.

---

[1]) *A.Kantz, R.Hofstadter* — Nucleonica, 1954, **12**(3), 36.
[2]) *Н.Л.Григоров, В.С.Мурзин, И.Д.Рапопорт* — ЖЭТФ, 1958, **34**, 506 (in Russian).
[3]) *V.S.Murzin* — Progress in El. Part. & Cosmic Ray Phys. Amsterdam, North Holl. Publ. Co., 1967, v.9, 245.
[4]) *В.С.Мурзин, Л.И.Сарычева.*є Космические лучи и их взаимодействие. -М.: Атомиздат, 1968. (in Russian).
[5]) *В.С.Мурзин, Л.И.Сарычева.* Множественные процессы при высоких энергиях. -М.: Атомиздат, 1974. (in Russian).
[6]) *H.R.Gustafson, L.W.Jones, M.J.Longo* — Proc. Int.Conf. Cosmic Rays. München, 1975, **9**, 3239.

We report here the data obtained in our cosmic ray experiment at mt. Aragatz with ionization calorimeter. The study focused on analysis of electromagnetic and hadronic cascade ***fluctuations*** as an observable manifestation of certain properties of "elementary" hadron-nucleus interaction. The apparatus used in this study was a 1,030 g/cm^2 thick iron absorber in which 16 layers of detectors (ionization chambers) were inserted every 65 g/cm^2 — over 300 detectors total. Additional 6 double layers of detectors separated with three 27 g/cm^2 lead filters atop of iron absorber and, above the calorimeter, a multilayer wire proportional counter and a hodoscopic array were used to distinguish showers induced by high energy electrons or photons, and hadrons — protons, pions or neutrons — and estimate the effect of nuclear fragments (target disintegration in inelastic collision) always present among the shower particles. The detailed description of the experimental equipment, complete representation of the methods used for the data analysis, and comprehensive discussion of the observed phenomena can be found in the book [7]). In this note we just remind in general outline the essence of the study and its basic results, that seem to be of interest nowadays.

---

[7]) *А.И.Демьянов, В.С.Мурзин, Л.И.Сарычева.*. Ядерно-каскадный процесс в плотном веществе. -М.: Nauka, 1977 (in Russian).

Analysis of Calorimeter Cascades

In each "elementary" hadronic interaction the *inelasticity* K (the fraction of energy lost by the projectile) strongly fluctuates; there may be quite few or many secondaries produced which carry away different portions of the transferred energy: some (neutral pions) immediately decay into photons, the others (charged pions and baryons, including the "persisting" projectile) afterwards interact in a random manner with the nuclei of the medium. Hence the apparent variety of hadronic cascades in a traditional (or old-fashioned) type calorimeter with optimum radiation to nuclear interaction length ratio for the absorber material $t_{rad}/\lambda_h \ll 1$, and corresponding longitudinal segmentation.

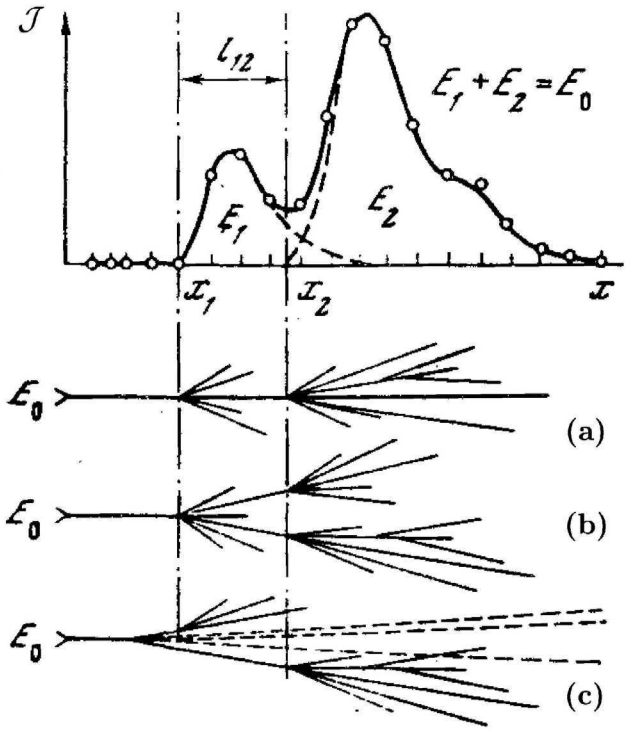

Fig. 1. A typical calorimeter cascade, and possible variants of its interpretation.

The cascade curve (ionization J versus depth x in absorber) may have one or several humps, their shape, size and disposition relative to the x-axis being different in every given event.

Every calorimeter cascade may be described by a set of basic parame-ters (see fig. 1): the number of humps in the cascade curve, or partial cascades i, the generation depth x_i of i-th partial cascade and its energy E_i (proportional to ionization it produces in all the involved detectors k^i, i.e $\sum J_k^i$), and the initial energy $E_0 = \sum E_i$ of incident hadron. There are other parameters substantial for better understanding of nuclear-cascade process (as e.g. the moments of a cascade curve $M_n = \sum k^n J_k / \sum J_k$, etc) as well as the auxiliary parameters used to investigate/estimate/correct for various systematic effects [7]), which we do not discuss here.

A careful analytical and Monte-Carlo calculations in terms of standard cascade model with regard for specific methodical effects (sporadic bursts of ionization due to nuclear disintegration distorting the shape of cascade curve, overlap of partial cascades generated too close to each other, limited depth of the absorber, etc) lead to a conclusion that the observable parameters of first and second (plus subsequent if any) partial cascades should in most cases be attributed to the properties of "elementary" interactions of a primary and a most energetic secondary (leading or persisting) hadron. In particular:

• The fraction of energy contained in the second (and subsequent) partial cascade(s), $E_2/E_0 = u$ characterizes the *elasticity* $1-K$ of first interaction in the given event. Within the region $0.3 \lesssim u \lesssim 0.9$ the observed spectrum $f(u)$ reproduces the true laboratory spectrum of leading hadrons L (if this spectrum is more or less flat or falling, as it follows from accelerator data for the reaction $pp \to p_L + X$ or $\to \pi_L + X$ respectively).

Direct measurements are that above 60 GeV pions constitute about 30% of the flux of cosmic ray hadrons at mountain-top level, however this does not affect the general picture of hadronic cascade behavior observed in the calorimeter: the spectrum $f(u)$ for leading pions from the reaction $\pi p \to \pi_L + X$ visibly falls in flat and steep components quite similar in shape to the spectrum of persisting nucleons and the spectrum of relatively soft secondary pions emerging from pp or incoherent pA collisions, thereby suggesting the same two production mechanisms (usually named *fragmentation* and *pionization*).

• The laboratory energy of a leading secondary $E_2 = \gamma_C\,(\tilde{E}_2 + \tilde{p}_2 \cos\tilde{\theta}_2)$, where $\tilde{E}_2$, $\tilde{p}_2$ and $\tilde{\theta}_2$ are its center-of-mass energy, momentum and emission angle, and γ_C is the Lorentz-factor of the center-of-mass reference frame (for *incoherent* production on a nucleus $\gamma_C \simeq \sqrt{E_0/2m_p}$). Thus, for relativistic case ($\tilde{E}_2 \simeq \tilde{p}_2$ and $\cos\tilde{\theta}_2 \simeq 1$) the ratio E_2/γ_C is a laboratory equivalent of the center-of-mass momentum $\tilde{p}_2$ of leading secondary. For non-relativistic case ($\tilde{p}_2 \ll \tilde{E}_2$) — say, a massive particle is born near the reaction threshold — the ratio $E_2/\gamma_C = m$ represents the mass of this particle.

If there is no any dramatic change in the behavior of the function $f(u)$ depending on E_0, the distribution E_2/γ_C can be obtained from the spectrum of primary cosmic ray hadrons and the spectrum of leading secondaries measured with the ionization calorimeter:

$$dN_{obs}(m) = \text{const} \int dN_{obs}(u)\, dN_{obs}(E_0) = \text{const} \int_{E_2^{min}}^{E_2^{max}} f\left(\frac{m^2}{2E_2}\right) \frac{dm}{m} \cdot F\left(\frac{2E_2^2}{m^2}\right) dE_2. \qquad (*)$$

(here m_p is set equal to 1).

• The generation depths x_1 and x_2 are distributed differently depending on whether the partial cascade is due to primary or secondary interaction. For the case of successive interactions of an incident hadron with interaction length λ (diagrams a or b in fig. 1):

$$\left.\begin{aligned} dN^S(x_1) &= e^{-x/\lambda} \cdot [\alpha(\Delta) - \delta(x_0)] \cdot \frac{dx}{\lambda}; \\ dN^S(x_2) &= \frac{l}{(l-\lambda)} \cdot [e^{-(x-\Delta)/l} - e^{-(x-\Delta)/\lambda}] \cdot \alpha(\Delta) \cdot \frac{dx}{l}. \end{aligned}\right\} \qquad (**)$$

(l is the mean free path for the second interaction).

If, for some reason, the point of first interaction is not seen (e.g. the energy transfer to the electromagnetic component is below the instrumental threshold) so that both partial cascades, E_1 and E_2 are in fact secondary (diagram c in fig. 1), the expected distributions

$$\left.\begin{aligned} dN^T(x_1) &= \frac{\Lambda}{(\Lambda-\lambda)} \cdot (e^{-x/\Lambda} - e^{-x/\lambda}) \cdot [\alpha(\Delta) - \delta(x_0)] \cdot \frac{dx}{L_1}; \\ dN^T(x_2) &= [\frac{L_2}{(L_2-\lambda)} \cdot (e^{-(x-\Delta)/L_2} - e^{-(x-\Delta)/\lambda}) \frac{\Lambda}{(\Lambda-\lambda)} \cdot (e^{-(x-\Delta)/\Lambda} - e^{-(x-\Delta)/\lambda})] \cdot \alpha(\Delta) \cdot \frac{dx}{L_2}. \end{aligned}\right\} (***)$$

where L_1 or L_2 is the interaction length of the secondary T_1 or T_2 which produces the partial cascade E_1 or E_2 respectively, and $1/\Lambda = 1/L_1 + 1/L_2$. In these formulas the factor $\alpha(\Delta) = e^{-\Delta/l}$ (or $e^{-\Delta/L_2}$) corrects for overlap of partial cascades if their generation depths x_1 and x_2 are within the minimum resolvable distance Δ, while the factor $\delta(x_0) = e^{-(x-x_0)/l}$ (or $e^{-(x-x_0)/L_2}$) accounts for possible loss of the partial cascade E_2 in a calorimeter of the limited *effective* depth x_0 (for $x_2 \gtrsim x_0$ the partial cascade cannot be reconstructed and/or its energy E_2 reliably estimated).

• The distribution of the parameter l depends on the average number $\langle n \rangle$ of secondaries contributing to the partial cascade E_2, and their interaction lengths.

For secondary nucleons and pions (interaction lengths $\sim\lambda$), the expected distribution

$$\boldsymbol{dN^S(l) = e^{-l/\langle l \rangle}\,\frac{dl}{\langle l \rangle}\cdot\varphi(x_0,l).} \qquad (****)$$

where $\langle l \rangle = \lambda/\langle n \rangle$, and the factor $\varphi(x_0,l) = 1 - e^{(l-x_0)/\lambda}$ appears because of the limited effective depth x_0 of the calorimeter absorber.

If $\langle n \rangle \simeq 1$, then $l = L$ and the function $f(u_L)$ is the pure spectrum of leading particles h_L. Otherwise, if $\langle n \rangle \neq 1$, the observable energy E_2 may be somewhat higher than the energy E_L of the leading particle h_L (e.g. persisting nucleon) proper. The resultant distortion of the observable function $f(u_L)$ for $u_L \gtrsim 0.3$ appears to be insignificant (due to steeply falling spectrum of numerous but relatively soft secondaries from *pionization* region) and may be easily corrected for.

For the "T-reaction" $\langle l \rangle = L_2$, and the factor φ in $(****)$ looks more complicated:

$$\varphi = \left[\, 1 - \frac{(\Lambda\, e^{(l-x_0)/\Lambda} - \lambda\, e^{(l-x_0)/\lambda})}{(\Lambda - \lambda)} \,\right] \cdot \frac{L_2}{(L_1 + L_2)},$$

the additional coefficient $L_2/(L_1 + L_2)$ reminding that the *numeration* of partial cascades E_1 and E_2 is not, in fact, arbitrary because L_1 and L_2 may be different.

Experimental results

The observable behavior of the parameters listed above was found to be at energies below 200 GeV in good agreement with what is expected for the standard cascade model, yet at higher energies it reveals certain irregularities of which the most important are:

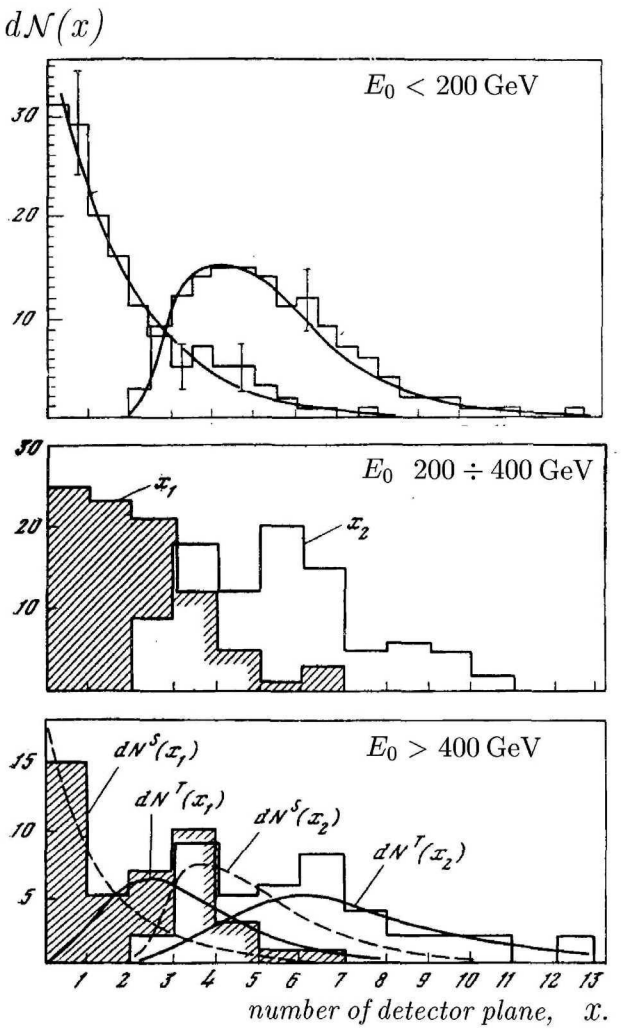

• Excess of partial cascades — both E_1 and E_2 — generated deep in the absorber: the approximation $(**)$ gives $P(\chi^2) < 0.01$. The best agreement with the experiment can be achieved assuming that some fraction of high energy events obeys this approximation, while for the others the generation depths x_1 and x_2 are distributed according to $(***)$ with the parameter $L_2 \simeq 2\lambda$ (fig. 2).

Fig. 2. Distribution of generation depths x_1 and x_2 of first and second humps of ionization in the calorimeter cascades of different energy.

Curves — expected distributions for standard cascade model (see diagram a or b in fig. 1), and for quasi-binary reaction pp or $pFe \to T_1 + T_2 + X_{soft}$ (diagram c in fig. 1).

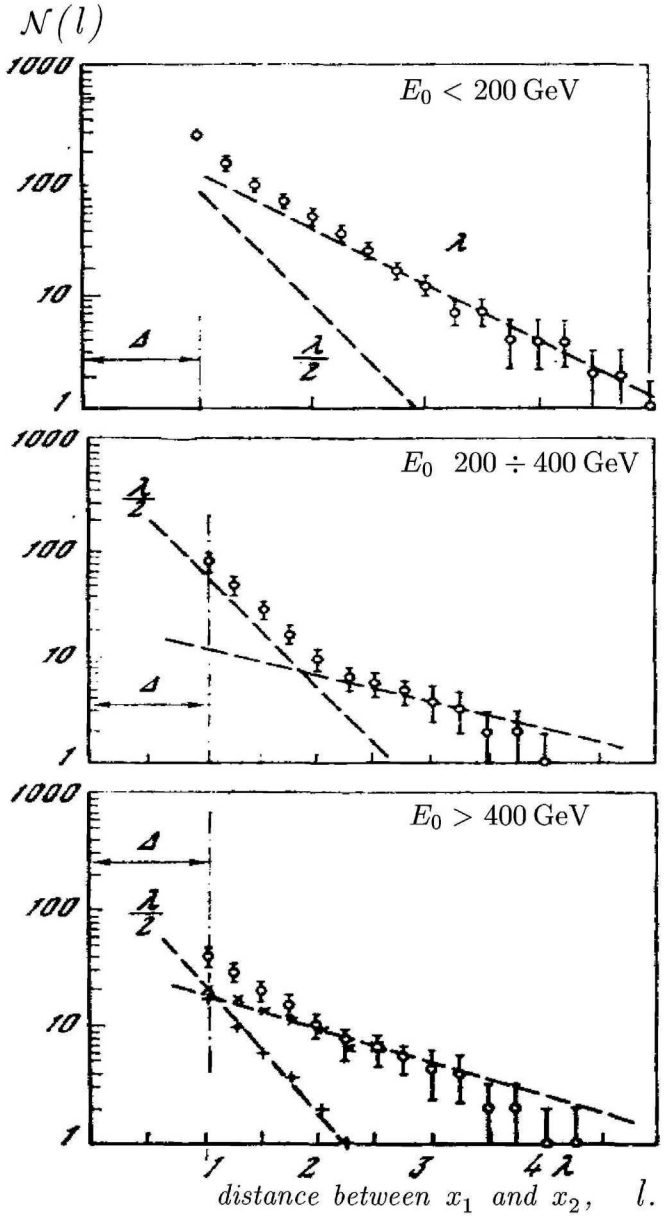

The distribution $(****)$ also changes its appearance about 200 GeV: at lower energies it may be fitted by an exponent with $\langle l \rangle \simeq 3/4\,\lambda$ (i.e. in 1/3 events $\langle n \rangle \simeq 2$) while at higher energies the distribution falls in two exponents — the steep one with $\langle l \rangle \sim \lambda/2$ and the flat one with $\langle l \rangle \simeq 2\lambda$, the "long range" component constituting a considerable fraction of events above 400 GeV (fig. 3).

Fig. 3. Distribution of distances l between generation depths x_1 and x_2 of first and second humps of ionization in the calorimeter cascades. Crosses mark distributions for regular cascades (+) and T-cascades (×).

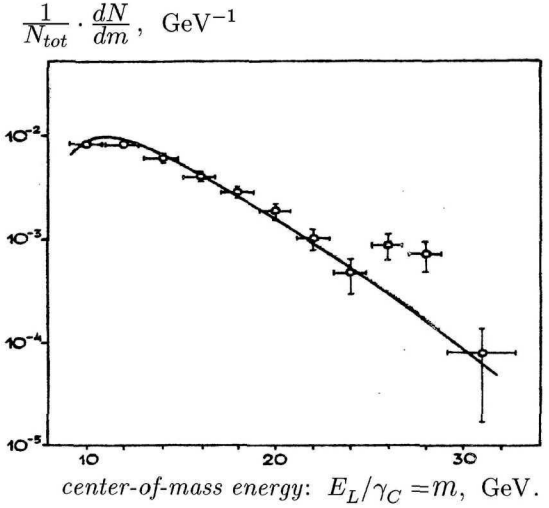

• Presence of a secondary L among the products of hadron-nucleus interaction, carrying away too large a portion E_L of the initial energy E_0 (fig. 4); and

Fig. 4. Spectrum of center-of-mass energies $m = E_L/\gamma_C$ of leading secondaries L for the cascades with $u_L > 0.5$.
Curve — the spectrum, obtained from $dN_{obs}(E_0)$ and $f_{obs}(u_L)$ measured in the same experiment.

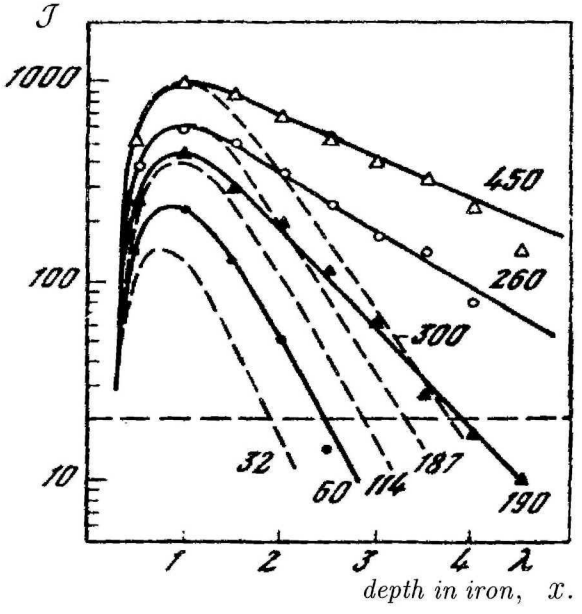

• Substantial slowing down of the energy absorption of the calorimeter cascade — partial cascades E_1 and E_2 in particular (fig. 5) — which is far beyond the predictions of standard cascade model.

Fig. 5. Average partial cascades E_1 and E_2 for T-events (solid curves) and for the rest events (dashed curves).
Number at each curve is the average energy in GeV of the corresponding group of partial cascades.

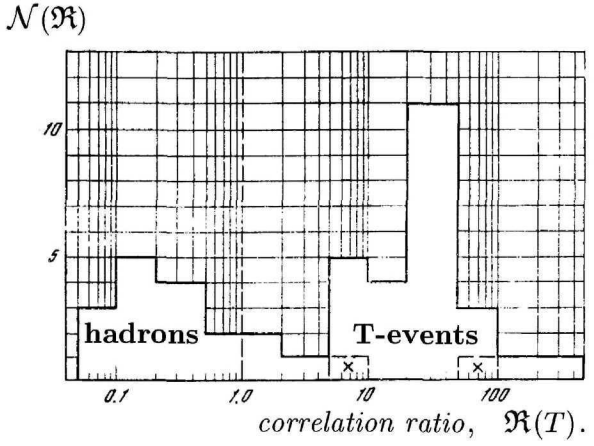

Fig. 6. Distribution of the correlation ratios $\mathfrak{R}(T)$ for the cascades of energy E_0 above 400 GeV.

Crosses (×) mark dubious T-events which fall out of angular distribution in fig. 8 ($\cos\tilde{\theta}_T > 1$).

The subsequent analysis of the experimental data has shown that all the mentioned irregularities are strictly correlated — i.e. arise due to one and the same group of events called "T-events". The correlation *ratios* $\mathfrak{R}(T)$ defined as

$$\mathfrak{R}(T) = \frac{w^T(x_1) \cdot w^T(x_2) \cdot w^T(E_2/\gamma_C)}{w^h(x_1) \cdot w^h(x_2) \cdot w^h(E_2/\gamma_C)}$$

distinctly group apart: regular hadrons on the left, T-events on the right of unity (fig. 6).

The functions $w^h(x_1)$, $w^h(x_2)$, $w^T(x_1)$ and $w^T(x_2)$ were calculated according to the forms (**) or (***) and fitted to the corresponding experimental distributions below and above 200 GeV; $w^h(E_2/\gamma_C)$ was obtained from the spectra $F(E_0)$ and $f(u)$ measured in the same experiment, while (a priory unknown) $w^T(E_2/\gamma_C)$ set constant.

As it is seen in fig. 6, the correlation is very strong: for the majority of events above 400 GeV the chances to be sorted in a wrong group are less than 0.01. Thereby the T-events are clearly separated from the rest (regular) hadronic cascades, making it possible to study the properties of a mechanism responsible for the observable effects. The characteristic features of this mechanism are:

- The T-cascades result from a sort of *binary* (or *quasi-binary*) reaction in which all (or nearly all) the interaction energy is transferred to the two secondary particles: pp or $pA \to T_1 + T_2$ $(+X_{soft})$.
- These T-particles are so massive that their appearance distorts the inclusive spectrum of center-of-mass energies for the leading secondaries emerging in the forward hemisphere.

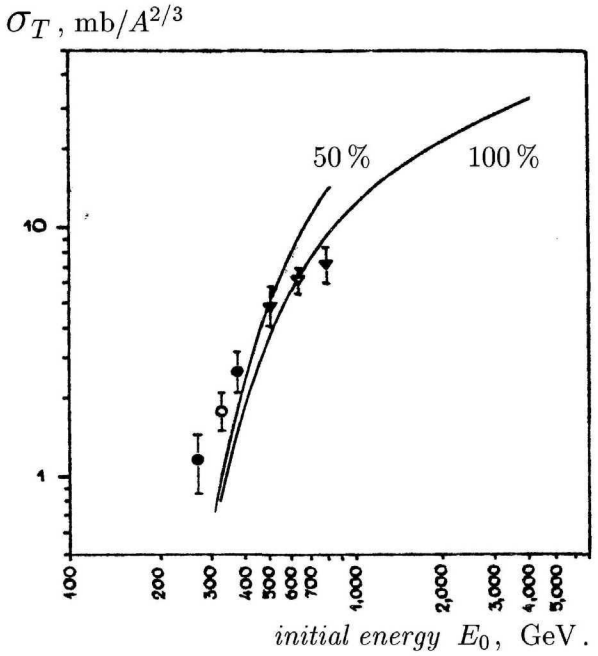

• The observed frequency of T-events corresponds to the T-production cross-section $\sigma_T(Fe)$ that at energies $\sim$1 TeV reaches few mb per "effective" nucleon, but steeply falls to zero near 200 GeV (fig. 7). Considering this energy as a kinematic threshold for the binary reaction, the mass of each T-particle appears to be $\sim$ 10 GeV/c^2.

Fig. 7. The observable cross-section for the reaction $p\,(n) + Fe \rightarrow T + T\ (+X_{soft})$ as a function of the initial energy E_0 of an incident nucleon.

Curves are calculated from the "knee" in the spectrum of primary cosmic ray nucleons $dN_{obs}(E_0)$, assuming 50 % and 100 % energy transfer to the massive penetrating secondaries.

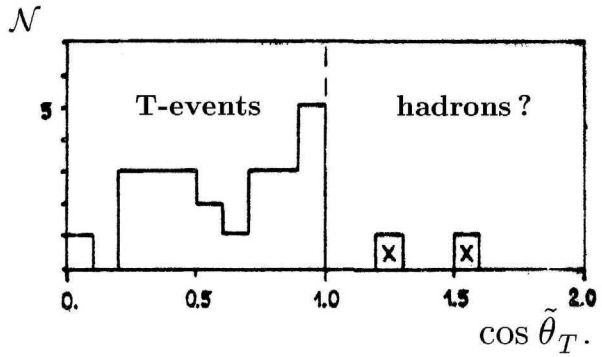

Fig. 8. Center-of-mass angular distribution for the binary reaction $pp \to T+T$, (M_T=10 GeV/c^2). Crosses (×) mark dubious T-events ($\cos\tilde{\theta}_T > 1$), — apparently regular yet seldom occurring fluctuations of the hadronic cascade [8]).

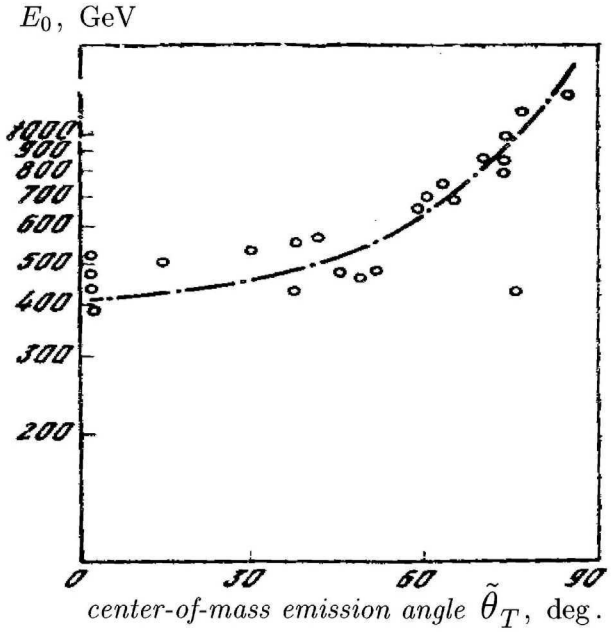

• For the binary reaction, the quantitative evaluation of the T-particle mass M_T allows calculating the center-of-mass production angle $\tilde{\theta}_T$ in each T-event. At a first sight the center-of-mass angular distribution looks more or less isotropic (fig. 8), however on closer examination it was found that near the reaction threshold the T-particles fly mostly forwards and backwards, with increasing energy the angles $\tilde{\theta}_T$ become larger and eventually group around 90° at $E_0 \sim 1$ TeV (fig. 9).

Fig. 9. Correlation between the total energy E_0 and the center-of-mass emission angle $\tilde{\theta}_T$ for T-cascades of energy E_0 above 400 GeV.

[8]) For the binary reaction $pp \to T_1 + T_2$, $\cos\tilde{\theta}_{T_2} = (E_{T_2} - E_{T_1})/(2\,\gamma_C\,[\,(m_p\,\gamma_C)^2 - M_T^2\,]^{\frac{1}{2}}) = -\cos\tilde{\theta}_{T_1}$. Setting $M_T = m_p$ displaces both the dubious events (×) properly, i.e. to the region $\cos\tilde{\theta}_T < 1$.

• The effective cross-section for the T-particle interaction in iron is substantially (by a factor of 2 or so) smaller than that of nucleons, provided that these particles are extraordinarily stable ($\tau_0^T \gg 10^{-9}\,\mathrm{sec}$) and always decay beyond the calorimeter. However the queer inclination of T-particles to fly at high energies across (in the center-of-mass reference frame) suggests an idea that their seemingly constant observable interaction length $\lambda_T \simeq 2\lambda_N$ results from the limited depth of the calorimeter. If the partial cascades in T-events E_1 and E_2 arise due do decays rather than interactions of T-particles, then

$$\langle l \rangle = c\,\langle (\tau_2^T - \tau_1^T) \rangle = c\,\tau_0^T \left(\frac{\langle E_2 \rangle}{M_T} - \frac{\langle E_1 \rangle}{M_T} \right)$$

the correlation between E_1 and E_2 being determined by $\tilde{\theta}_T$. Hence:

$$\langle l \rangle = c\,\tau_0^T \cdot \frac{\langle E_0 \rangle}{M_T} \cdot \langle \cos\tilde{\theta}_T \rangle \quad \left(\text{assuming } \frac{M_T}{m_N^2 \gamma_C^2} \ll 1 \right).$$

In other words, decreasing of $\langle \cos\tilde{\theta}_T \rangle$ as the inverse $\langle E_0 \rangle$ should result in the constant observable $\langle l \rangle$ just if the latter is the mean T-particle *decay* path, i.e. $\langle l \rangle \propto \langle E_0 \rangle$. The angular distribution in fig. 8 appears to be in good agreement with the decay model [9]): the values of τ_0^T obtained for the different energy bins coincide within few percent around the average $\tau_0^T = 0.8 \cdot 10^{-10}\,\mathrm{sec}$.

• The decay model provides natural explanation for the rapid decrease with increasing energy E_0 of the rate of energy deposition by a hadronic cascade in the calorimeter as a result of relativistic prolongation of T-particle life. The same effect observed for partial cascades E_1 and E_2, produced in the calorimeter by each T-particle (unlike regular hadrons), may be indicative of a cascade mode of T-particle decay.

• The lifetime $\tau_0^T \simeq 10^{-10}\,\mathrm{sec}$ implies that with increasing energy more and more of T-particles decay beyond the calorimeter, esp. those emitted in forward center-of-mass direction, thereby escaping the observation. Hence above 1 TeV we should not expect the same typical of T-reaction effects as listed above. The analysis of interaction depths, viz. x_1 as applied to the *observable* cascade curves with one hump, taken alone is not much informative:

[9]) The coefficient of correlation between l and E_2 is 0.47 ± 0.25 for T-cascades and 0.00 ± 0.06 for "non-T"-cascades. For the decay model (linear dependence $\langle l \rangle$ of E_2 and exponential distribution (****) for each E_2) the expected value is 0.45.

without distinct correlation with behavior of other parameters the T-events will very likely be missed among the rest (regular) hadronic cascades. The *instrumental selection* of T-events with $\tilde{\theta}_T \to \pi/2$, or $f(u) \to 0.5 = \text{const}$, makes the resultant distribution $E_2/\gamma_C = m$ essentially a reproduction of the spectrum E_0:

$$dN_{obs}(m) = \text{const} \int dN_{obs}(u)\, dN_{obs}(E_0) \to \text{const} \cdot N_{obs}(E_0)\, dm$$

which adds nothing special to the distribution $dN_{obs}(m)$ for regular hadrons. In this case the spectrum $f(u)$ may become slightly more bulging near $u \sim 0.5$, yet such an effect in itself allows various interpretations without any allusion to the T-process.

On the other hand, the *loss* of most energetic events associated with T-particle production must distort the spectrum E_0 measured by the calorimeter, mainly for the cascades with $u > 0.5$. Indeed, in the experiment performed with a similar calorimeter with larger aperture in order to collect sufficient statistics above 1 TeV the analysis of cascade curves reveals no noticeable effects characteristic of T-events, however the spectra $N_{obs}(E_0) \sim E_0^{-\beta}$ for the cascades with $u > 0.5$ are noticeably more steep than for all the cascades: $\beta_{u>0.5} = 3.57 \pm 0.12$ as compared to $\beta_{tot} = 3.27 \pm 0.07$ (in the energy region 100 GeV to 1 TeV these two spectra practically coincide). For the T-particles with mass $\simeq 10\,\text{GeV}$ and lifetime $\simeq 10^{-10}\,\text{sec}$ the decay path $\lambda_d^T \sim x_0$ near 1 TeV so that they can now and again escape the calorimeter; near 10 TeV $\lambda_d^T \gtrsim 10\, x_0$, i.e. $\gtrsim 90$ percent of T-particles should be lost. Assuming the production cross-section $\sigma_T(Fe)$ approximately constant above 1 TeV and the index of *true* energy spectrum of incident hadrons $\beta^* \simeq 3.2$, the observable change of the index β due to loss of T-particles appears to be just $\Delta\beta = (\beta_{obs} - \beta^*) = 0.3$ in agreement with the experiment.

Discussion

Generally speaking, there are known physical processes that may in principle be responsible for appearance of such kind of "anomalous" effects as those observed in our experiment, or at least some of them. It is worth mentioning here the so called *diffraction dissociation* (coherent or incoherent) on nuclei. The characteristic features of diffraction production are low multiplicity and strong collimation of secondaries in forward direction. In the diffraction type reaction, e.g. $pA \to p\pi^+\pi^- + A$ (or A^*), the interaction point is not seen in the calorimeter unless its detectors are sensitive enough to identify a single relativistic particle. The rapid growth with energy of the cross-section for this

channel would result in excess of events with large E_2/γ_C due to the attribute of diffraction irregularity in the leading proton spectrum $f(u_L)$ of the form $1/(1-u_L)$. The diffraction dissociation, however, does not explain large $\langle l \rangle$ of secondaries, nor too slow and energy dependent absorption rate of partial cascades they produce in the calorimeter absorber, nor why the "anomalies" disappear above 1 TeV.

Strange hadrons, K-mesons and hyperons Λ/Σ etc, have the appropriate lifetime $(10^{-9} \div 10^{-11})$ and interaction length (viz. $\lambda_K \sim 1/2\lambda_N$), but the other effects, including distinct energy threshold ~ 200 GeV for generation of "anomalous" cascades, may hardly be associated with the strange particle production.

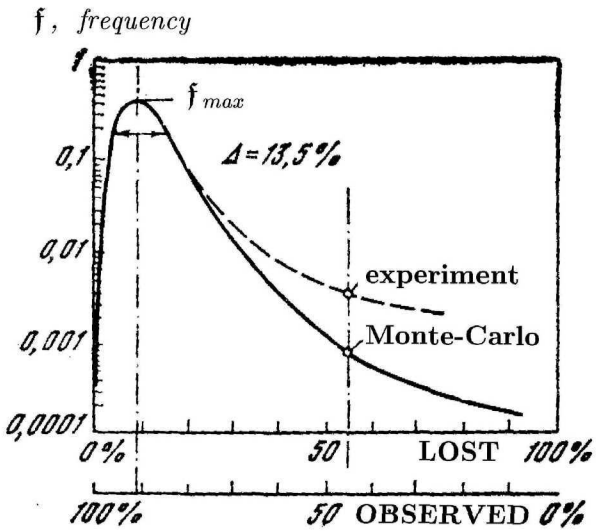

Fig. 10. Fraction of initial energy E_0, (LOST or OBSERVED) in a calorimeter with iron absorber $\simeq 7\lambda$ hick and 30 planes of scintillation detectors.
Solid curve: Monte-Carlo simulation for the standard cascade model;
Dashed curve: experiment in a beam of 300 GeV protons.

The model of T-particles described here is a purely empirical construction, invented in order to describe (as consistent as possible) the effects we observed experimentally — no *theoretical* considerations were used about the mechanism of the T-process. On the phenomenological plane, this model offers a reasonable interpretation of the number of unusual, or unexpected observations made in other experiments. A typical example presents the experiment on calibration of a calorimeter $\sim 7\lambda$ thick performed at Fermilab in the beam of 300 GeV protons[6]). The obtained calibration curve $f(E_{obs}/E_0)$ had a maximum about 0.9 and a long tail extending to 0, i.e. in many cases nearly all the energy escapes the calorimeter. Monte-Carlo simulation in terms of standard cascade model gives the calibration curve which coincides with the experimental one down to $E_{obs}/E_0 \sim 0.7$; in the region of large losses increasing divergence between the two curves is observed: for $E_{obs}/E_0 = 0.5$ the experimental curve runs already 5 times as high as Monte-Carlo predicts (fig. 10).

Another observation that can be described even *quantitatively* basing on our T-model is the apparent "knee" in the spectrum of primary cosmic ray hadrons *measured* with a relatively shallow (some 3λ) calorimeter orbiting the Earth [10]). The curves figuring in fig. 7 were calculated in [11]) assuming that the *observable* "knee" in the primary spectrum appears due to an unknown interaction mechanism in which a large portion (50 % or 100 %) of the energy E_0 is transferred to massive and highly penetrating secondary particles escaping the calorimeter. At last, the model of T-particles may perhaps relate to — or help to specify — the conception of "strangelets" [12]) that has become pretty popular since recently.

Conclusion

The cosmic ray observations, if they report unexpected effects, may seem intriguing yet seldom too much convincing: the low flux of high energy cosmic ray radiation (hence low statistics) combined with very limited input information and intricate often indirect considerations used for data interpretation make such observations somewhat ambiguous.

Nevertheless, a brief description of our cosmic ray experiment, principles and methods of the calorimeter data analysis presented in this note illustrates the potentialities of the calorimeter technique which may find applications to accelerator experiments. In a thick enough ($\sim 10\lambda$) calorimeter with e.g. tungsten absorber ($t_{rad}/\lambda \simeq 0.03$), optimum longitudinal and transverse segmentation (thus high spatial resolution) and detectors type proportional wire chambers (insusceptible to radiation damage and, unlike scintillation or Čerenkov counters, ensuring correct measurement of the energy of nuclear fragments — i.e. *compensated* spectrometry), the behavior of partial cascades produced in *every* interaction of *each* energetic incident/secondary particle provides a valuable additional information hardly accessible using any other such compact an apparatus.

• **In particular, calorimeters like CASTOR or ZDC in the CMS experiment at LHC seem adaptable for the study of "exotics" similar to that observed in our cosmic ray experiment which is described here. (Forward Region Layout)**

---

[10]) *Л.Н.Басилова и др.* — Изв. АН СССР, сер. физ., 1967, **31**, 1505 (in Russian).
[11]) *L.Kaufmann, Y.R.Mongan* — Phys. Rev., 1970, **11**, 988.
[12]) see e.g.: *E.Gladysz-Dziadus* — Phys. Part. & Nucl., 2003, **34**, 286; and references therein.